Available online at www.sciencedirect.com
SCIENCE DIRECT®
Journal of Solid State Chemistry 178 (2005) 3476–3484
JOURNAL OF SOLID STATE CHEMISTRY
www.elsevier.com/locate/jssc

# Phase relationships in the pseudo-binary 2(ZnTe)-$CuInTe_2$ system

Liudmila Roussak*, Gerald Wagner, Susan Schorr, Klaus Bente

*University of Leipzig, Faculty of Chemistry and Mineralogy, Institute of Mineralogy, Crystallography and Materials Science, Linnéstrasse 3-5 (TA), D-04103 Leipzig, Germany*

Received 23 March 2005; received in revised form 29 August 2005; accepted 3 September 2005
Available online 5 October 2005

**Abstract**

Subsolidus phase relationships in the $2(ZnTe)_x(CuInTe_2)_{1-x}$ system were investigated by TEM experiments combined with EDX analysis. The samples were prepared by the solid-state reaction of the elements during long annealing times, followed by either quenching in ice-cold water, or by controlled cooling at different rates. Using the chemical compositions of single and coexisting phases at various temperatures, the boundaries of the two-phase region have been determined. At room temperature, the two-phase region extends from $x = 0.10$ to 0.31. For $x < 0.10$ only mixed crystals with tetragonal structure exist. Between $x = 0.31$ and 1 alloys with the cubic structure are stable.

The morphology of the tetragonal domains and their orientation relationship to the cubic matrix were determined by SAD, TEM and HRTEM experiments. The tetragonal phase embedded within the cubic matrix has a flat ellipsoidal shape, whose short axis coincides with the tetragonal *c*-axis. The three topotaxial orientation relationships between the tetragonal domains and the surrounding cubic matrix were found to be: $[001]_{tetr.}\|[100]_{cub.}$, $[001]_{tetr.}\|[010]_{cub.}$ and $[001]_{tetr.}\|[001]_{cub.}$. There is an indication that the nucleation starts from small regions displaying cation ordering according to the CuPt-type structure. Reaching the two-phase equilibrium, the tetragonal domains as well as the surrounding cubic phase are free of this cation ordering.


*Keywords:* Phase diagram; Electron microscopy; Alloys of ZnTe/$CuInTe_2$; Order–disorder

## 1. Introduction

$2(ZnTe)_x(CuInTe_2)_{1-x}$ alloys are materials of potential interest in photovoltaic applications [1,2]. They are formed by the combination of binary sphalerite-type ZnTe and ternary chalcopyrite-type $CuInTe_2$. The band gap energies of the $2(ZnTe)_x(CuInTe_2)_{1-x}$ alloys (so-called ZCIT) vary from 0.97 eV for pure $CuInTe_2$ to 2.23 eV for ZnTe [3]. Depending on the chemical composition and temperature the $2(ZnTe)_x(CuInTe_2)_{1-x}$ alloys can form mixed crystals with tetragonal chalcopyrite-type (SG $I\bar{4}2d$) or cubic sphalerite-type structure (SG $F\bar{4}3m$) [3,4]. On the other hand, if the non-isotype $C^{II}X$ and $A^{I}B^{III}X_2$ materials ($A$ = Cu, Ag; $B$ = Ga, In; $C$ = Zn, Cd; $X$ = S, Se, Te) are mixed, a concentration region can be observed, where both tetragonal and cubic phases coexist (two-phase field) [5,6]. For the system under study, $2(ZnTe)_x(CuInTe_2)_{1-x}$, Garbato and Ledda [4] have found a wide two-phase field (miscibility gap) between $0.1 < x < 0.33$ at room temperature (RT), whereas Gallardo [7] reported the existence of a complete solid solution series. According to the experimental data published by Bodnar et al. [3,8], the $2(ZnTe)_x(CuInTe_2)_{1-x}$ system exhibits extended regions of solid solutions in which alloys exclusively with the tetragonal chalcopyrite and cubic sphalerite structure exist. The two-phase field expands between $0.3 < x < 0.4$ only.

For applications in photovoltaic devices a controllable adjustment of the stoichiometry of $2(ZnTe)_x(CuInTe_2)_{1-x}$ is required as single crystals, thin films as well as homo- and hetero-junctions in order to achieve the desired structural and physical properties. Therefore, a detailed understanding of the two-phase field and the extent of its stability is necessary.

The aim of this work is to specify the boundaries of the two-phase region at RT as well as its temperature dependence. Despite a recent study in which the change of the lattice parameters upon the mixing of ZnTe and

*Corresponding author. Fax: +1 49 341 9736 642.
*E-mail address:* roussak@rz.uni-leipzig.de (L. Roussak).

0022-4596/$ - see front matter © 2005 Elsevier Inc. All rights reserved.
doi:10.1016/j.jssc.2005.09.003

$CuInTe_2$ has recently been published [9], there is no detailed information about the structure, morphology or the orientational relationship of both (cubic and tetragonal) phases. Therefore, the study of the nucleation and growth kinetics of the tetragonal phase, which is enveloped by the cubic matrix, can provide new insights for the understanding of the diffusion processes at the interfacial region of hetero-structures such as substrate/$CuInTe_2$/ZnTe necessary for device fabrication.

## 2. Experimental

$2(ZnTe)_x(CuInTe_2)_{1-x}$ alloys were pre-synthesized by the solid-state reaction of the pure elements (5 N) in evacuated quartz tubes at 800 °C. After homogenization at 700 °C for 60 days, the samples were cooled to RT at a cooling rate of about 42 K/h. This was then ground once more in an agate mortar and pressed into tablets. Thereafter two kinds of heat treatment were carried out:

(1) Long-time annealing of samples followed by a quenching in ice-cold water was chosen to determine the temperature and composition dependence of the two-phase field width (so-called equilibrium experiments). After this treatment the chemical compositions of the domains and matrix are assumed to be close to that of equilibrium (near-equilibrium concentration).
(2) Controlled cooling experiments applying different cooling rates were carried out to check the effect on the deviation of the chemical composition from those at equilibrium (kinetic experiments). Moreover, these samples should provide information about the nucleation and growth kinetics of the tetragonal domains.

For the equilibrium experiments samples with $x = 0.05$, 0.10, 0.15 and 0.20 were placed in sealed evacuated quartz ampoules and heated with a rate of 10 K/h from RT to 730 °C. This was followed by an annealing for 30 h. Thereafter, the samples were cooled down at 10 K/h to the desired final temperatures $T_{hom}$ and annealed to reach equilibrium. Both $T_{hom}$ and the period $t$ (days) of annealing are given in Table 1. To prevent the loss of tellurium during annealing a small amount Te was added into the ampoules (1 wt%). Afterwards the samples were quenched in ice-cold water.

The $2(ZnTe)_x(CuInTe_2)_{1-x}$ samples with an average composition of $x = 0.05$, 0.10, 0.15, 0.20 and 0.25 used for kinetic experiments, were treated in the same way as described above. However, the final annealing was performed at 605 °C for 20 days followed by a cooling down to RT at rates of 2, 5, 10, 15 and about 42 K/h (see Table 2).

Based on both literature reports (cf. [4]) and our own experience, the particular chemical compositions detailed above were chosen as the two-phase-field is expected to occur in this $x$-region.

The as-treated polycrystalline material was prepared for transmission electron microscopy by mechanical grinding, polishing by ion milling at 4 kV, a beam current of 0.5 mA and a beam incidence angle of 11–13°. The TEM and high-resolution TEM (HRTEM) experiments were carried out in a Philips CM 200 STEM electron microscope equipped with a super twin objective lens (point resolution 0.23 nm). The EMS-software [10] was employed to simulate the selected area diffraction (SAD) patterns for the different structures and superstructures. An adapted EDX-system was used to determine the chemical composition of the tetragonal domains and cubic matrix as well as the average composition (large beam diameter). The precise determination

Table 1
Annealing temperature, annealing period and chemical compositions measured by TEM-EDX

| Nominal 2(ZnTe) content (mol%) | $T_{hom.}$ (°C) | $t_{hom.}$ (days) | Average chemical composition TEM-EDX | Composition of tetragonal phase (domains) | Composition of cubic phase (matrix) |
|---|---|---|---|---|---|
| 5 | 605 | 17 | $Zn_{0.055}Cu_{0.492}In_{0.452}Te$ | $Zn_{0.030}Cu_{0.490}In_{0.480}Te$<br>$Zn_{0.041}Cu_{0.491}In_{0.468}Te$<br>$Zn_{0.057}Cu_{0.485}In_{0.457}Te$ | $Zn_{0.109}Cu_{0.452}In_{0.438}Te$ |
| 10 | 605 | 25 | n.d. | $Zn_{0.084}Cu_{0.429}In_{0.487}Te$<br>$Zn_{0.098}Cu_{0.439}In_{0.463}Te$ | $Zn_{0.109}Cu_{0.401}In_{0.481}Te$ |
| 10 | 605 | 40 | $Zn_{0.092}Cu_{0.447}In_{0.461}Te$ | $Zn_{0.060}Cu_{0.440}In_{0.501}Te$ | $Zn_{0.094}Cu_{0.445}In_{0.467}Te$ |
| 10 | 555 | 18 | $Zn_{0.099}Cu_{0.449}In_{0.451}Te$ | $Zn_{0.048}Cu_{0.477}In_{0.476}Te$ | $Zn_{0.108}Cu_{0.444}In_{0.447}Te$ |
| 10 | 455 | 31 | | $Zn_{0.090}Cu_{0.498}In_{0.411}Te$ | $Zn_{0.184}Cu_{0.457}In_{0.358}Te$ |
| 10 | 355 | 60 | $Zn_{0.086}Cu_{0.457}In_{0.460}Te$ | $Zn_{0.086}Cu_{0.457}In_{0.460}Te$ | |
| 15 | 555 | 18 | $Zn_{0.143}Cu_{0.444}In_{0.413}Te$ | n.d. | $Zn_{0.143}Cu_{0.444}In_{0.413}Te$ |
| 15 | 455 | 31 | n.d. | $Zn_{0.086}Cu_{0.453}In_{0.461}Te$ | $Zn_{0.172}Cu_{0.412}In_{0.417}Te$ |
| 15 | 355 | 60 | n.d. | $Zn_{0.105}Cu_{0.448}In_{0.449}Te$ | $Zn_{0.248}Cu_{0.378}In_{0.367}Te$ |
| 15 | 300 | 60 | n.d. | $Zn_{0.097}Cu_{0.419}In_{0.484}Te$ | $Zn_{0.279}Cu_{0.329}In_{0.392}Te$ |
| 20 | 300 | 60 | n.d. | $Zn_{0.123}Cu_{0.402}In_{0.475}Te$ | $Zn_{0.279}Cu_{0.313}In_{0.407}Te$ |

All samples were quenched at $T_{hom.}$ in ice-cold water. n.d. means that the chemical composition could not be detected because of the very small size of domains and their overlapping. In this case it was not possible to determine precisely the composition of the cubic phase too. Therefore, the average composition was attributed to the main phase, i.e. cubic phase.

Table 2
Heat treatment conditions (annealing temperature, annealing period, cooling rate) and chemical compositions measured by TEM-EDX

| Nominal 2(ZnTe) content (mol%) | $T_{hom.}$ (°C) | $t_{hom.}$ (days) | Cooling rate (K/h) | Average chemical composition TEM-EDX | Composition of tetragonal phase (domains) | Composition of cubic phase (matrix) |
|---|---|---|---|---|---|---|
| 25 | 605 | 40 | 2 | $Zn_{0.244}Cu_{0.387}In_{0.37}Te$ | $Zn_{0.128}Cu_{0.420}In_{0.452}Te$ | $Zn_{0.312}Cu_{0.334}In_{0.354}Te$ |
| 25 | 605 | 20 | 10 | n.d. | $Zn_{0.099}Cu_{0.436}In_{0.466}Te$ | $Zn_{0.293}Cu_{0.329}In_{0.379}Te$ |
| 20 | 605 | 40 | 2 | $Zn_{0.194}Cu_{0.399}In_{0.405}Te$ | $Zn_{0.116}Cu_{0.427}In_{0.456}Te$ | $Zn_{0.299}Cu_{0.333}In_{0.368}Te$ |
| 20 | 605 | 20 | 5 | $Zn_{0.164}Cu_{0.395}In_{0.441}Te$ | $Zn_{0.112}Cu_{0.421}In_{0.467}Te.$ | $Zn_{0.286}Cu_{0.338}In_{0.376}Te$ |
| 20 | 605 | 20 | 10 | $Zn_{0.185}Cu_{0.414}In_{0.401}Te$ | $Zn_{0.119}Cu_{0.436}In_{0.445}Te$ | $Zn_{0.2898}Cu_{0.35}In_{0.360}Te$ |
| 20 | 605 | 20 | 15 | $Zn_{0.181}Cu_{0.412}In_{0.407}Te$ | $Zn_{0.120}Cu_{0.435}In_{0.445}Te$ | $Zn_{0.286}Cu_{0.344}In_{0.370}Te$ |
| 20 | 605 | 20 | 42 | $Zn_{0.179}Cu_{0.411}In_{0.411}Te$ | $Zn_{0.117}Cu_{0.430}In_{0.453}Te$ | $Zn_{0.268}Cu_{0.351}In_{0.381}Te$ |
| 15 | 605 | 40 | 2 | $Zn_{0.153}Cu_{0.432}In_{0.415}Te$ | $Zn_{0.113}Cu_{0.443}In_{0.445}Te$ | $Zn_{0.313}Cu_{0.341}In_{0.346}Te$ |
| 15 | 605 | 20 | 10 | $Zn_{0.143}Cu_{0.448}In_{0.409}Te$ | $Zn_{0.112}Cu_{0.458}In_{0.430}Te$ | $Zn_{0.299}Cu_{0.361}In_{0.340}Te$ |
| 15 | 605 | 20 | 15 | $Zn_{0.151}Cu_{0.417}In_{0.431}Te$ | $Zn_{0.124}Cu_{0.419}In_{0.457}Te$ | $Zn_{0.291}Cu_{0.338}In_{0.371}Te$ |
| 15 | 605 | 20 | 42 | $Zn_{0.147}Cu_{0.419}In_{0.435}Te$ | $Zn_{0.100}Cu_{0.436}In_{0.464}Te$ | $Zn_{0.254}Cu_{0.355}In_{0.392}Te$ |
| 10 | 605 | 20 | 5 | n.d. | $Zn_{0.083}Cu_{0.437}In_{0.481}Te$<br>$Zn_{0.114}Cu_{0.422}In_{0.464}Te$ | $Zn_{0.283}Cu_{0.33}In_{0.387}Te$ |
| 10 | 605 | 20 | 10 | n.d. | $Zn_{0.090}Cu_{0.486}In_{0.424}Te$<br>$Zn_{0.122}Cu_{0.462}In_{0.417}Te$ | $Zn_{0.291}Cu_{0.370}In_{0.340}Te$ |
| 5 | 605 | 40 | 2 | $Zn_{0.031}Cu_{0.481}In_{0.487}Te$ | $Zn_{0.031}Cu_{0.481}In_{0.487}Te$ | |
| 5 | 605 | 20 | 10 | $Zn_{0.188}Cu_{0.408}In_{0.404}Te$ | $Zn_{0.121}Cu_{0.432}In_{0.447}Te$ | $Zn_{0.293}Cu_{0.342}In_{0.365}Te$ |
| 27.5[a] | 700 | 29 | 5 | $Zn_{0.374}Cu_{0.352}In_{0.274}Te$ | | $Zn_{0.374}Cu_{0.352}In_{0.274}Te$ |
| 27.5[a] | 700 | 29 | 5 | $Zn_{0.317}Cu_{0.330}In_{0.352}Te$ | | $Zn_{0.317}Cu_{0.330}In_{0.352}Te$ |
| 35[a] | 700 | 29 | 5 | $Zn_{0.400}Cu_{0.321}In_{0.278}Te$ | | $Zn_{0.400}Cu_{0.321}In_{0.278}Te$ |
| 40[a] | 700 | 29 | 5 | $Zn_{0.394}Cu_{0.302}In_{0.304}Te$ | | $Zn_{0.394}Cu_{0.302}In_{0.304}Te$ |
| 5[a] | 700 | 29 | 5 | $Zn_{0.053}Cu_{0.470}In_{0.477}Te$ | $Zn_{0.053}Cu_{0.470}In_{0.477}Te$ | |

[a]Samples were grown from the melt. n.d.—not detectable—means, due to the extremely inhomogeneous distribution of the domains, that it was not possible to measure the average composition.

of the chemical composition of the two phases, i.e. the independent composition of the tetragonal and the surrounding cubic phases, was performed with a spot diameter of only 5–10 nm (STEM nano-probe mode). By using standard stoichiometric samples such as ZnTe, $Cu_2Te$, $In_2Te_3$ and $CuInTe_2$ the Cliff–Lorimer factors $k_{AB}$ were calibrated. From this procedure it was possible to determine the 2(ZnTe) concentration in $2(ZnTe)_x(CuInTe_2)_{1-x}$ with an accuracy of $\pm 1.0$ mol%.

## 3. Results and discussion

Regardless of the treatment of the samples, i.e. long-time annealing or controlled cooling, the shape and orientational relationship of tetragonal domains to the matrix, remain unchanged. Remarkable differences only exist in their size.

### 3.1. Structure and orientation relationship between the tetragonal domains and cubic matrix

Within the two-phase field ranging at RT from $0.10 \leqslant x \leqslant 0.31$, TEM indicates that the tetragonal phase always appears as sliced ellipsoids which are arranged on a rectangular grid (cf. Fig. 1). Due to the related crystal structure and the extremely small misfit between the tetragonal domains and the surrounding cubic matrix, their boundaries are nearly strain-free and are therefore without any dislocations. TEM dark-field imaging and SAD of the domains, reveal a defined orientational relationship as can be seen in Fig. 1. The domains imaged in Fig. 1 with beam direction (bd) close to the [001] were found in a sample with a nominal composition $Zn_{0.20}Cu_{0.40}In_{0.40}Te$. As can be seen in the SAD patterns, the crystallographic axes of the tetragonal and cubic phases coincide, where the tetragonal $c$-axis always lies parallel to the short axis of the disc. The three topotaxial orientation relationships between the tetragonal domains and the surrounding cubic matrix are represented by the SAD patterns in Fig. 1b–e.

Fig. 2 schematically outlines the possible orientations of the tetragonal phase (domains) within the cubic matrix. The crystallographic relations between the tetragonal domains and cubic matrix established in this work are: $[001]_{tetragonal} \| [100]_{cubic}$, $[001]_{tetragonal} \| [010]_{cubic}$ and $[001]_{tetragonal} \| [001]_{cubic}$. However, all SAD patterns originating from domains reveal additional spots on the positions of the chalcopyrite structure (SG $I\bar{4}2d$) relating to forbidden 0 0 2 and 1 1 0 reflections (encircled in Fig. 1). Comparing experimental SAD pattern with the simulated ones for the different structures and superstructures, both with and without cation ordering, it is evident that the additional spots observed can be assigned to the ordering of metal atoms, as for the stannite structure (SG $I\bar{4}2m$). The existence of this metastable structure in the $(CX)_{2x}(ABX_2)_{1-x}$ systems has already been theoretically predicted [11–13]. It appears that the phase transition from the chalcopyrite to the sphalerite structures proceeds via the intermediate metastable stannite phase. It should be noted that the stannite-type cation ordering appears more

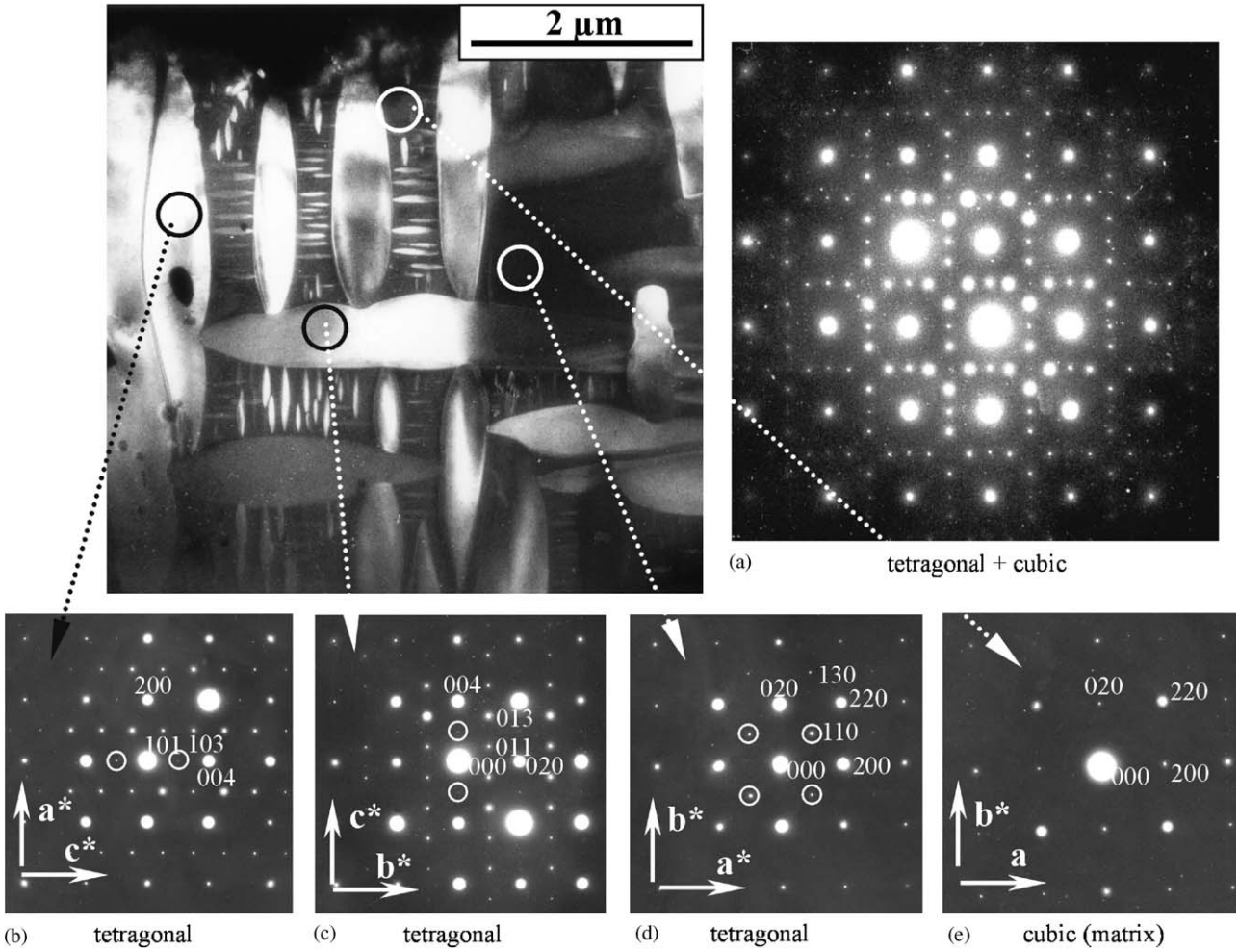


Fig. 1. TEM dark-field image and SAD patterns of differently oriented tetragonal domains (b–d) and cubic matrix (e). The compositions of the domains and matrix are $Zn_{0.123}Cu_{0.402}In_{0.475}Te$ and $Zn_{0.279}Cu_{0.313}In_{0.407}Te$, respectively. The SAD pattern taken from the multi-domain region (a) is a superposition of all patterns (b–e). Beam direction (bd) close to [001]. The encircled spots in (b–d) are caused by a stannite-type cation ordering.

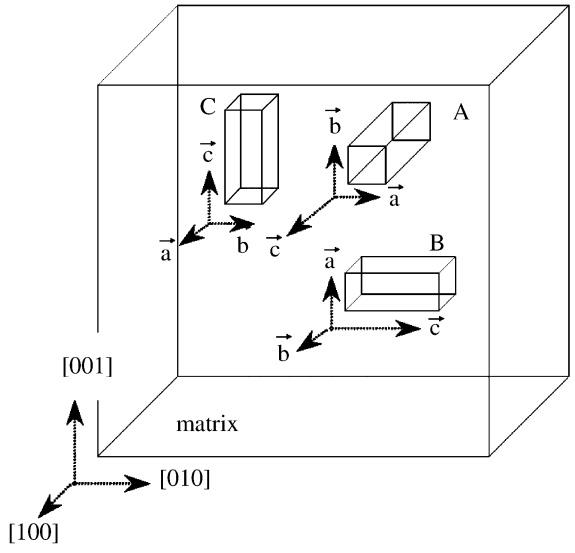


Fig. 2. Schematically drawn possible observed orientations. *C*: $[001]_{cub.}//[001]_{tetr.}$; *B*: $[010]_{cub.}//[001]_{tetr.}$ and *A*: $[100]_{cub.}//[001]_{tetr.}$

distinctly in samples being far from the equilibrium state. The SAD patterns from the matrix having only diffraction spots being typical for the sphalerite structure (SG $F\bar{4}3m$) appear (see Fig. 1e).

### 3.2. Nucleation of the tetragonal domains within the cubic matrix

In order to obtain additional information about the origin of the tetragonal phase, we studied a polycrystalline sample with an average composition $Zn_{0.10}Cu_{0.449}In_{0.451}Te$ (Fig. 3). By doing so, the 2(ZnTe) content in $2(ZnTe)_x(CuInTe_2)_{1-x}$ is assured to be close to the boundary between the two-phase field and the tetragonal single-phase region. This sample was annealed at 555 °C for 18 days and then quenched in ice-cold water to freeze-in the small domain nuclei as these would develop into larger domains upon slow cooling. TEM experiments indicated that during the initial stage of the phase separation, the tetragonal domains develop from tiny regions (10–20 nm)

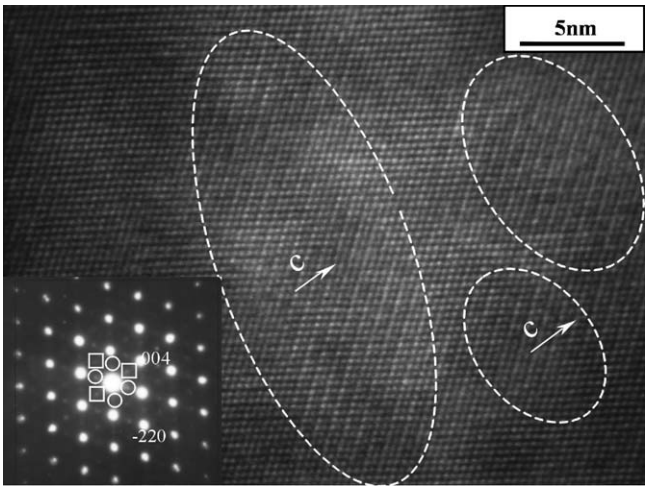


Fig. 3. HRTEM image of tiny regions having cation ordering (encircled) inside the matrix. These limited regions seem to act as nuclei for the formation of the tetragonal domains. As found by SAD (beam direction parallel to [110]), the regions exhibit a stannite-like structure (marked by open squares) and reveal ordering of the metal atoms according to the CuPt-type structure. In the SAD pattern this ordering causes additional spots on the positions $1/2[2\bar{2}1]^*$ and $1/2[\bar{2}21]^*$ (encircled). The average sample composition is $Zn_{0.10}Cu_{0.449}In_{0.451}Te$.

having CuPt-type ordering of the Zn, Cu and In. The corresponding HRTEM image taken from the matrix reveals double periodicity in contrast of the {112} lattice planes, as shown in Fig. 3. The CuPt-type ordering is confirmed by the observation of the extra spots on the $1/2[2\bar{2}1]^*$ and $1/2[\bar{2}21]^*$ positions in the SAD pattern (encircled).

Moreover, the diffraction pattern reveals spots at 0 0 2 and $\bar{1}$ 1 0 positions too (marked with squares in Fig. 3) which are actually forbidden for the chalcopyrite-type structure but can be attributed to a stannite-like structure of the tetragonal domains. HRTEM measurements established that the *c*-axis of these tiny regions (enclosed by dotted lines) is aligned with the *c*-axis of the large tetragonal domains which would develop during long annealing times and/or controlled cooling.

If the small tetragonal domains were allowed to develop into larger ones by annealing/slow cooling, it was found they are infected by CuPt-ordering. However, the superstructure reflections become weaker the closer the samples approach to the equilibrium state under long annealing times. They are completely absent in samples at the equilibrium state.

### 3.3. Phase diagram

The phase diagram shown in Fig. 4 only reflects results from TEM-EDX experiments carried out at samples of nominal compositions $x = 0.05$, 0.10, 0.15, 0.20 and 0.25. As confirmed there is a wide two-phase region. Its width changes with temperature and 2(ZnTe) content in $2(ZnTe)_x(CuInTe_2)_{1-x}$, as can be taken from Table 1 and Fig. 4, where the dotted lines terminate the two-phase field.

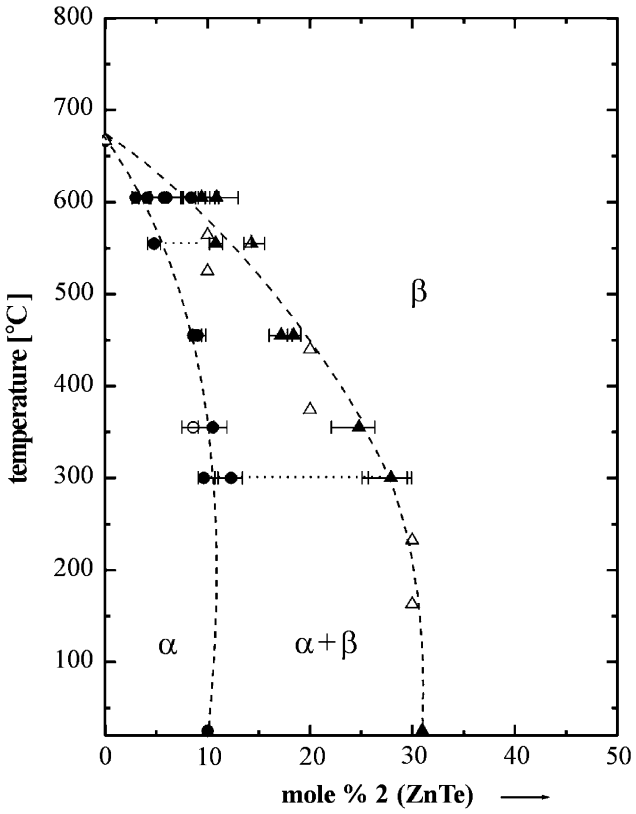


Fig. 4. Subsolidus region of the $2(ZnTe)_x(CuInTe_2)_{1-x}$ system as revealed by TEM-EDX analysis. The temperatures are afflicted with an error of $\pm 10$ K. $\alpha$ denotes the chalcopyrite-type structure and $\beta$ means sphalerite-type structure. Inside the field $\alpha + \beta$ tetragonal domains and cubic matrix coexist. Open triangles—data taken from Bodnar et al. [8], filled triangles—cubic matrix, filled circles—tetragonal domains, open circles—tetragonal single-phase, filled square—average 2(ZnTe) content: domains exist, but their composition is not detectable.

In the temperature range from 300 to 550 °C the boundaries of the two-phase field can be precisely defined. In this range the chemical composition of the domains, as well as the matrix of the $2(ZnTe)_x(CuInTe_2)_{1-x}$ alloys, is found to be stoichiometric with respect to the Cu/In ratio (almost unity) in both the tetragonal and cubic phase (see Table 1). At $T > 605$ °C, the compositional limits cannot be defined reliably (see Fig. 4), as no single-phase material could be obtained under these *T*-*x*-conditions independent of the annealing time (cf. Table 1). However, in the particular case of a $Zn_{0.092}Cu_{0.447}In_{0.461}Te$ alloy with an increased annealing period of about 40 days, solely the tetragonal domains and the surrounding matrix exist (see Table 1). These results indicate that the annealing of samples for around 40 days is necessary to reach a near-equilibrium state at 605 °C. Hence, the appreciable scattering of the domain and matrix compositions at this temperature (as shown in Fig. 4) should be caused by the non-equilibrium state. Additionally, it cannot be excluded that more than two phases, possibly including other metastable and unknown phases, exist in this *T*-*x*-region.

In the low-temperature region, for samples annealed at 300 °C over 60 days and then quenched, a third phase could

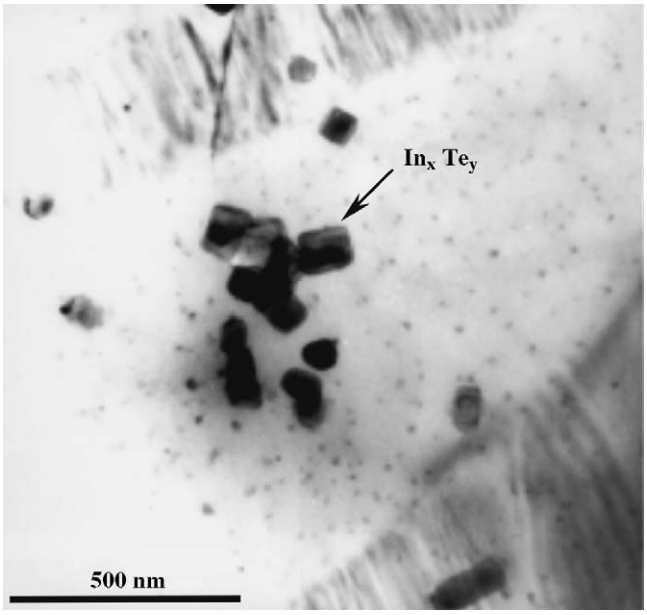


Fig. 5. TEM bright-field image of the long-time annealed (60 days) sample confirming the presence of $In_xTe_y$ precipitates (size 50–100 nm). They appear as dark rectangular contrasts. The annealing temperature and nominal chemical composition are 300 °C and $Zn_{0.20}Cu_{0.40}In_{0.40}Te$. The compositions of the tetragonal domains and cubic matrix are $Zn_{0.123}Cu_{0.402}In_{0.475}Te$ and $Zn_{0.279}Cu_{0.313}In_{0.407}Te$.

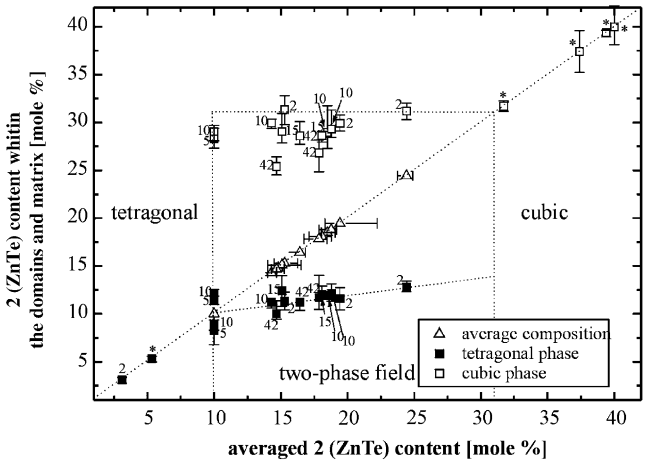


Fig. 6. The extent of the two-phase region for room temperature as obtained from TEM-EDX measurements for slowly cooled samples. The cooling rate is indicated by the numbers attached.

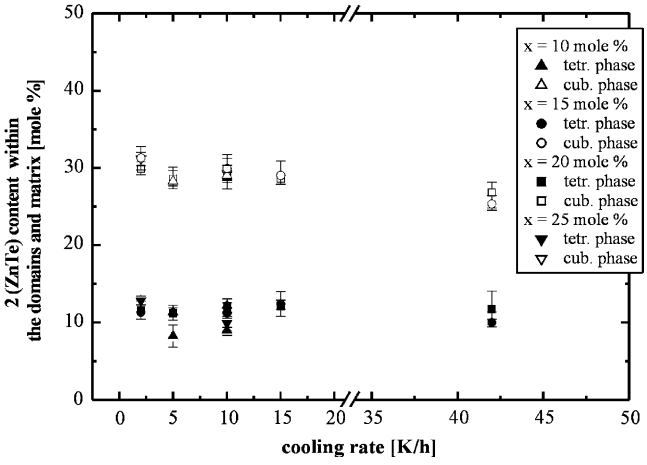


Fig. 7. 2(ZnTe) content of the tetragonal domains and cubic matrix versus cooling rate for samples of nearly equal average composition (cf. Table 2). It was assumed that for a cooling rate of zero the equilibrium concentration is achieved.

be detected. The TEM and TEM-EDX measurements (see Fig. 5) have established that this randomly localized phase represents $In_xTe_y$ with $x/y$ ratios ranging from 1 to 3.5, but the majority of this phase was found to be indium rich. This phase can be found in the tetragonal domains as well as in the cubic matrix. However, in contrast to the tetragonal domains ($\alpha$-phase) which are topotaxially ingrown into the surrounding cubic matrix ($\beta$-phase), there is no orientational relationship of the $In_xTe_y$ to either the domains or to the matrix.

To determine the near-equilibrium compositions of the domains and the matrix for RT the samples which underwent a controlled cooling have been analysed by TEM-EDX. The results are shown and listed in the Figs. 6 and 7 and Table 2. Data in Fig. 6 reveal that above all, the composition of the cubic matrix deviates more from the dashed line (near-equilibrium concentration) as the cooling rate increases. Assuming the domain growth is controlled by diffusion, the equilibrium concentrations cannot be reached at low temperatures by applying high rates of cooling.

From the TEM images of the samples, the non-equilibrium state is readily recognized by the presence of very small domains located between the larger ones. The dissolution of these extremely small tetragonal domains and the associated preferred diffusion of Cu and In towards the larger domains (the majority of Zn-atoms remain in the matrix) during the long annealing times, determine the equilibrium and/or non-equilibrium state of the samples. As confirmed by TEM the area (matrix) between the large domains is free of these small domains if the samples are sufficiently close to, or at, the equilibrium state. Therefore, the samples which undergo a controlled cooling can never be in equilibrium. However, cooling with 2 K/h produced samples in which the composition of the domains and the matrix should be near to the equilibrium values. To demonstrate the increased deviation from equilibrium more quantitatively, the 2(ZnTe) contents in both the domains and the matrix were determined for samples of nearly equal average composition, but with different cooling rates (see Fig. 7). As already demonstrated in Fig. 6 the compositions become closer to the equilibrium value as the cooling rate decreases. Fig. 7 clearly indicates that a decrease of the cooling rate leads to the increase of the 2(ZnTe) content in the cubic phase. In the case of the tetragonal phase, this will be increasingly depleted of Zn. For a cooling rate of zero the equilibrium concentration should be achieved. By extrapolation of the experimental data given in Fig. 7 the near-equilibrium

2(ZnTe) concentrations at RT were found to be $x = 0.10$ for the tetragonal domains and $x = 0.31$ for the cubic matrix. Hence, the region of the two-phase field in the $2(ZnTe)_x(CuInTe_2)_{1-x}$ system at RT is limited to the chemical composition range $0.10 \leqslant x \leqslant 0.31$.

This experimentally determined extent of the two-phase field is in accord with that already published by Garbato and Ledda [4], who specified a two-phase field width of $0.10 < x < 0.33$.

### 3.4. Effect of anion and cation substitution on the width and compositional location of the two-phase field

Based upon new data concerning the compositional limits of the two-phase field and their temperature dependence determined by TEM-EDX [6,14,15], we compared the $2(ZnTe)_x(CuInTe_2)_{1-x}$, $2(ZnSe)_x(CuInSe_2)_{1-x}$ and $2(ZnS)_x(CuInS_2)_{1-x}$ systems, where only the anion is changed. Including $2(ZnS)_x(CuGaS_2)_{1-x}$ as a system where the cation is additionally exchanged, we try to give a plausible explanation for the shrinkage of the two-phase field with increasing radius of the anion. As shown in Table 3 the boundary concentration where the $\alpha$-phase field ends and the two-phase field starts is for all $X$ about 10 mol% 2(Zn$X$). $X$ means S, Se and Te. However, with increasing atomic radius of $X$, i.e. $r_S^{2-} < r_{Se}^{2-} < r_{Te}^{2-}$, the boundary concentration, which marks the transition from the two-phase field to the $\beta$-phase field, decreases considerably.

Since the crystal structure of the ternary $ABX_2$ alloys (SG $I\bar{4}2d$) is closely related to that of the $CX$ compounds (SG $F\bar{4}3m$), where their unit cell represents a doubled sphalerite unit cell in the $z$-direction, it can be assumed that the deviation of the ratio of the tetragonal lattice parameters ($c/a$ ratio) of the Cu$In X_2$ alloys from its ideal value of 2, can be correlated to the above mentioned shrinkage. According to Refs. [16,17], there is a direct correlation between the radii and $c/a$. Therefore in the following we have made use of only $c/a$. The more the $c/a$ value deviates from 2 for a particular chalcopyrite-like compound, the more its solubility in Zn$X$ is decreased. Subsequently the two-phase field enlarges and the region where the cubic phase is stable shrinks.

A similar behaviour is observed when cations have been exchanged but the anion $X$ remains unchanged (cf. [18]). Then, the solid solubility of the chalcopyrite-like Cu$BX_2$ in sphalerite-like Zn$X$ alloys is expected to be larger when the cation radius enlarges too. Thus, the region of the solid solutions with cubic structure should be broader in the systems containing larger cations or anions. However, as seen in Table 3, the experimentally determined $x$-values for the change $\alpha + \beta \Rightarrow \beta$ given in the literature deviate appreciably. All data given in the literature and which were measured by DTA seem to be incorrect. Since we are sure that the TEM-EDX data (footnote a in Table 3) determined by [14,15,19] and given in this work are correct, the lines in Fig. 8 provide a credible correlation. The influence of cation and anion substitution (represented by

Table 3
Limits of the two-phase field at room temperature for the $2(ZnX)_x(CuInX_2)_{1-x}$ and $2(ZnX)_x(CuGaX_2)_{1-x}$ systems, where $X$ = S, Se and Te

| System | Radius of the anion $X^2$ (pm) [20] | $c/a$ ratio of $CuInX_2$ or $CuGaX_2$ | Concentration $x$ of 2(ZnX) for $\alpha \Rightarrow \alpha + \beta$ | Concentration $x$ of 2(ZnX) for $\alpha + \beta \Rightarrow \beta$ or $\alpha \Rightarrow \beta$ | Ref. |
|---|---|---|---|---|---|
| $2(ZnS)_x(CuInS_2)_{1-x}$ | 184 | 2.016 | $0.10 \pm 0.01$[a] | $0.41 \pm 0.01$[a] | [6,14] |
| | | | | *0.19* | [21] |
| | | 2.023 | | *0.33* | [18] |
| | | | | *0.20* | [22] |
| | | | | *0.25* | [7] |
| | | | 0.29 | 0.43 | [23] at 580 °C |
| $2(ZnSe)_x(CuInSe_2)_{1-x}$ | 198 | 2.008 | $0.10 \pm 0.01$[a] | $0.36 \pm 0.01$[a] | [15] |
| | | | 0.43 | 0.48 | [7] |
| | | | | *0.6* | [28] |
| | | 2.010 | 0.3 | 0.4 | [24,25] |
| $2(ZnTe)_x(CuInTe_2)_{1-x}$ | 221 | 2.000 | $0.10 \pm 0.01$[a] | $0.31 \pm 0.01$[a] | This work |
| | | | 0.10 | 0.33 | [4] |
| | | | | *0.3* | [7] |
| | | 2.000 | 0.3 | 0.4 | [3,8] |
| $2(ZnS)_x(CuGaS_2)_{1-x}$ | 184 | | $\approx 0.17$[a] | $\approx 0.48$[a] | [19] |
| | | 1.958 [26] | | $\approx$ *0.50* | [18,27] |
| | | | | $\approx$ *0.25* | [7] |
| $2(ZnSe)_x(CuGaSe_2)_{1-x}$ | 198 | 1.961 | | *0.40* | [28] |
| $2(ZnTe)_x(CuGaTe_2)_{1-x}$ | 221 | | 0.25 | 0.35 | [7] |
| | | 1.986 | 0.275 | 0.4 | [5] |

$\alpha \Rightarrow \alpha + \beta$ and $\alpha + \beta \Rightarrow \beta$ mean that a two-phase field exists. $\alpha \Rightarrow \beta$ means that a direct change from the tetragonal ($\alpha$) to the cubic phase ($\beta$) only was reported.

[a]The 2(ZnX) concentrations determined by TEM-EDX experiments.

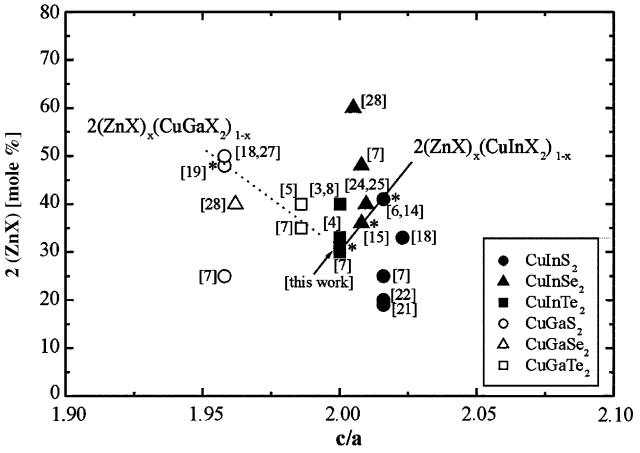


Fig. 8. Variation of the boundary concentration, which marks the transition from the two-phase field ($\alpha+\beta$) to the $\beta$-phase field in the $2(ZnX)_x(CuInX_2)_{1-x}$ and $2(ZnX)_x(CuGaX_2)_{1-x}$ systems, where $X=$ S, Se and Te, versus the $c/a$ ratio of the $CuInX_2$ and $CuGaX_2$ alloys, respectively. The $2(ZnX)$ concentrations determined by TEM-EDX experiments are marked *.

$c/a$) on the solid solubility of the $ABX_2$ in $CX$ for two homologous rows, i.e. $2(ZnX)_x(CuInX_2)_{1-x}$ and $2(ZnX)_x(CuGaX_2)_{1-x}$, where $X=$ S, Se and Te is shown in Fig. 8 and confirms our assumption that the miscibility gap, here particularly represented by the transition $\alpha+\beta \Rightarrow \beta$, decreases approaching the ideal value $c/a=2$. The largest cubic region occurs in the telluride systems independent of the kind of cation. Consequently, the smallest two-phase field exists also for the telluride systems.

However, comparing $2(ZnS)_x(CuGaS_2)_{1-x}$ with $2(ZnS)_x(CuInS_2)_{1-x}$, $2(ZnSe)_x(CuGaSe_2)_{1-x}$ with $2(ZnSe)_x(CuInSe_2)_{1-x}$ and $2(ZnTe)_x(CuGaTe_2)_{1-x}$ with $2(ZnTe)_x(CuInTe_2)_{1-x}$ in the system containing the larger cation ($r^{3+}_{Ga}=47$ pm and $r^{3+}_{In}=62$ pm [20]) the extent of the two-phase field is more distinctly influenced by the cations rather than anions.

## 4. Conclusion

We have shown that TEM experiments combined with EDX analysis represent a unique method for the detailed study of the complex phase diagrams, especially in the subsolidus region. By a critical review of the DTA data published in the literature, it is apparent that such measurements seem not to be suitable to determine the phase transitions in that region. Therefore, the extent of the two-phase field in the $2(ZnTe)_x(CuInTe_2)_{1-x}$ system has been determined by TEM-EDX which allows one to measure the chemical composition in a restricted area (beam diameter about 5 nm) located both inside the domains as well as the matrix.

At room temperature the two-phase field extends between $x=0.10$ and 0.31. In this composition range a tetragonal and cubic phase coexist. The morphology and orientational relationship between the coexisting tetragonal domains and cubic matrix in $2(ZnTe)_x(CuInTe_2)_{1-x}$ have been characterized in more detail. TEM experiments proved that the tetragonal phase with the shape of a flat disc is embedded in the cubic matrix. There is a distinct crystallographic relationship where the tetragonal domains are simultaneously arranged on the (100), (010) and (001) planes. The short axis of the disc-shaped domains and tetragonal $c$-axis coincide. It was found that during the initial stage of the phase separation the nucleation of domains is stimulated via tiny regions having CuPt-type ordering of the cations Zn, Cu and In.

The change of the compositional and structural properties of the $2(ZnTe)_x(CuInTe_2)_{1-x}$ alloys in dependence of the temperature, 2(ZnTe) content and the kind of heat treatment (long annealing time, controlled cooling) were also studied. It was established that the near-equilibrium state and, hence, the equilibrium concentration inside the domains and matrix could be obtained exclusively by long-time annealing and/or applying cooling rates less than 2 K/h. At higher cooling rates (rapid cooling), the 2(ZnTe) concentration within $2(ZnTe)_x(CuInTe_2)_{1-x}$ can deviate appreciably from that of equilibrium.

## Acknowledgments

Mrs. M. Peter is greatly appreciated for preparing TEM samples. Kindly, I.V. Bodnar and coworkers have supplied some melt-grown samples too.

## References

[1] L.L. Kazmerski, Y.J. Juang, J. Vac. Sci. Technol. 14 (1977) 769–776.
[2] J.L. Shay, J.H. Wernick, Ternary Chalcopyrite Semiconductors: Growth, Electronic Properties and Applications, Pergamon Press, Oxford, 1975.
[3] I.V. Bodnar, A. Eifler, Th. Doering, W. Schmitz, K. Bente, V.F. Gremenok, I.A. Victorov, V. Riede, Cryst. Res. Technol. 35 (2000) 1135–1140.
[4] L. Garbato, F. Ledda, J. Solid State Chem. 30 (1979) 189–195.
[5] P. Manca, L. Garbato, Sol. Cells 16 (1986) 101–121.
[6] S. Schorr, G. Wagner, J. Alloy Compd. 396 (2005) 202–207.
[7] P.G. Gallardo, Phys. Stat. Sol. (a) 134 (1992) 119–125.
[8] I.V. Bodnar, B.V. Korzun, L.V. Chibusova, Russ. J. Inorg. Chem. 45 (2000) 1405–1408.
[9] S. Schorr, M. Tovar, D. Sheptyakov, L. Keller, G. Geandier, J. Phys. Chem. Sol. (2005) in press.
[10] P.A. Stadelmann, Ultramicroscopy 21 (1987) 131–145.
[11] K.E. Newman, X. Xiang, Phys. Rev. B 44 (1991) 4677–4680.
[12] R. Osório, Z.W. Lu, S.H. Wei, A. Zunger, Phys. Rev. B 47 (1993) 9985–9988.
[13] J. Ni, S. Iwata, Phys. Rev. B 52 (1995) 3214–3219.
[14] G. Wagner, F. Fleischer, S. Schorr, J. Crystal Growth 283 (2005) 356–366.
[15] G. Wagner, S. Lehmann, S. Schorr, unpublished.
[16] J. Noolandi, Phys. Rev. B 10 (1974) 2490–2494.
[17] J.E. Jaffe, A. Zunger, Phys. Rev. B 29 (1984) 1882–1906.
[18] M. Robbins, M.A. Miksovsky, J. Solid State Chem. 5 (1972) 462–466.
[19] S. Schorr, D. Göricke, G. Wagner, unpublished.
[20] R.D. Shannon, Acta Crystallogr. A 32 (1976) 751–767.
[21] K. Bente, Th. Doering, Chem. Erde 51 (1991) 291–295.

[22] C. Sombuthawee, S.B. Bonsall, F.A. Hummel, J. Solid. State Chem. 25 (1978) 391–399.
[23] O.V. Parasyuk, S.V. Voronyuk, L.D. Gulay, G.Y. Davidyuk, V.O. Halka, J. Alloy Compd. 348 (2003) 57–64.
[24] I.V. Bodnar, I.A. Victorov, I.V. Chibusova, Inst. Phys. Conf. Ser. 152 (1997) 119–122.
[25] I.V. Bodnar, V.F. Gremenok, W. Schmitz, K. Bente, Th. Doering, Cryst. Res. Technol. 39 (2004) 301–307.
[26] H. Hahn, G. Frank, W. Klingler, A. Meyer, G. Storger, Z. Anorg. Allg. Chem. 271 (1953) 153–170.
[27] E.F. Apple, J. Electrochem. Soc. 105 (1958) 251–255.
[28] V.G. Lamprecht, Mater. Res. Bull. 8 (1973) 1383–1388.